Effects of Denaturants on the Dynamics of Loop Formation in Polypeptides

Marco Buscaglia, Lisa J. Lapidus, William A. Eaton, and James Hofrichter
Laboratory of Chemical Physics, National Institute of Diabetes and Digestive and Kidney Diseases, National Institutes of Health, Bethesda, Maryland 20892-0520

ABSTRACT   Quenching of the triplet state of tryptophan by close contact with cysteine has been used to measure the reaction-limited and diffusion-limited rates of loop formation in disordered polypeptides having the sequence cys-(ala-gly-gln)$_j$-trp ($j = 1$–9). The decrease in the length-dependence of the reaction-limited rate for short chains in aqueous buffer, previously attributed to chain stiffness, is not observed at high concentrations of chemical denaturant (6 M GdmCl and 8 M urea), showing that denaturants increase chain flexibility. For long chains, both reaction-limited and diffusion-limited rates are significantly smaller in denaturant and exhibit a steeper length dependence. The results can be explained using end-to-end distributions from a wormlike chain model in which excluded volume interactions are incorporated by associating a 0.4–0.5 nm diameter hard sphere with the end of each virtual peptide bond. Fitting the data with this model shows that the denaturants reduce the persistence length from ~0.6 nm to ~0.4 nm, only slightly greater than the length of a peptide bond. The same model also describes the reported length dependence for the radii of gyration of chemically denatured proteins containing 50–400 residues. The end-to-end diffusion coefficients obtained from the diffusion-limited rates are smaller than the sum of the monomer diffusion coefficients and exhibit significant temperature dependence, suggesting that diffusion is slowed by internal friction arising from barriers to backbone conformational changes.

INTRODUCTION

An understanding of how proteins fold must incorporate experimental and theoretical descriptions of the kinetics and dynamics of the elementary processes that occur in polypeptide chains (1). The formation of a loop to produce an intramolecular contact in an unfolded sequence is, perhaps, the simplest of these processes. We have recently demonstrated that the long-lived triplet state of tryptophan formed by nanosecond optical excitation can be used as a probe for measuring the rate of loop formation (2,3). When tryptophan is positioned at one end of a disordered polypeptide and cysteine at the other, measurement of the triplet decay monitors the formation of a contact between the tryptophan and cysteine. Since quenching by cysteine at contact is not instantaneous, the rate observed experimentally is less than the rate of contact formation, and the chain can sample a significant fraction of the equilibrium distribution of end-to-end distances before quenching occurs. The measurements therefore allow the dependence of this distribution on peptide length and solution conditions to be determined. Moreover, since cysteine is the only naturally occurring amino acid that efficiently quenches the tryptophan triplet state (4), this probe can be utilized to investigate a specific intramolecular contact for any sequence containing a single

tryptophan and cysteine. Recently, it has been shown that this approach can be used to measure contact formation in unfolded proteins (5) and to measure the unfolding rates for fast-folding proteins (6).

Intramolecular contact to form a disordered loop can, to a good approximation, be described by the simple two-step kinetic model shown in Fig. 1. In this model, the ends of the peptide first diffuse together with rate k_{D+} to form an encounter complex; the cysteine then either quenches the tryptophan triplet state with rate q or diffuses away with a rate k_{D-}. The observed quenching rate (k_{obs}) is given by

$$k_{obs} = k_{D+} \frac{q}{k_{D-} + q} \equiv k_{D+} \phi, \qquad (1)$$

where the quenching yield, ϕ, is the probability of quenching during the lifetime of the encounter complex.

Diffusion-limited rates can be obtained by measuring the dependence of the quenching rates on solution viscosity. Equation 1 can be rearranged to give

$$\frac{1}{k_{obs}} = \frac{1}{k_R} + \frac{1}{k_{D+}}, \qquad (2)$$

where $k_R = qK_{eq}$ is the reaction-limited rate, and K_{eq} ($\equiv k_{D+}/k_{D-}$) is the equilibrium constant for forming the encounter complex. If $k_{D-} \gg q$, quenching is reaction-limited and this expression becomes

$$k_R = \frac{k_{D+}}{k_{D-}} q \equiv K_{eq} q. \qquad (3)$$

The reaction-limited rate, k_R, is that measured when diffusion is sufficiently fast ($k_{D-} \gg q$) that the encounter
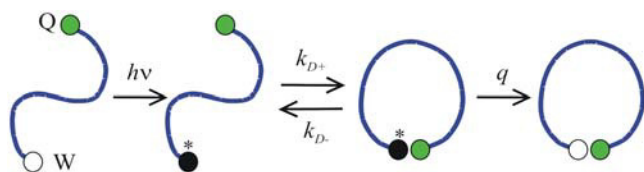
FIGURE 1 Scheme for measuring the rate of contact formation between tryptophan and cysteine at the ends of a random polypeptide. Pulsed excitation leads to population of the lowest excited triplet state of tryptophan. Tryptophan can then contact cysteine in a diffusion-limited process k_{D+}. During the lifetime of this contact pair, quenching of the triplet occurs with a probability determined by the quenching rate and the rate of diffusive dissociation of the contact pair.

complex is formed and broken several times before quenching ($\phi \ll 1$) so the population of unquenched molecules forming encounter complexes is in equilibrium with the complete ensemble of chain conformations. Since k_R depends only on the distribution of end-to-end distances in the unfolded chain and q, it provides a novel probe of this ensemble. For example, increasing the average end-to-end distance by increasing chain length or by swelling the chain via repulsive interactions will decrease K_{eq} and therefore decrease k_R. The diffusion-limited rate, k_{D+}, is the measured rate when $q \gg k_{D-}$, and corresponds to the rate of bringing the ends together to form a short-range contact. Diffusion-limited rates can be obtained by measuring the dependence of the quenching rates on solution viscosity. By plotting $1/k_{obs}$ versus solution viscosity, $1/k_R$ is obtained from the intercept at zero viscosity and the diffusion limited time for contact formation, $1/\eta k_{D+}$, is obtained from the slope. Interpretation of k_{D+} is less straightforward since it depends both on the end-to-end distribution and on the diffusional dynamics of the chain ends.

Because the quenching rate is dependent on distance (7), the encounter complex is not sharply defined, and a somewhat more complex analysis is required to take this into account. With a distance-dependent quenching rate, $q(x)$, Wilemski and Fixman (8) showed that k_{obs} (Eq. 1) can be approximated as

$$\frac{1}{k_{obs}} = \frac{1}{k_R} + \frac{1}{k_R^2} \int_0^\infty \langle \delta q(t) \delta q(0) \rangle dt, \qquad (4)$$

where

$$k_R = \langle q \rangle = \int_a^{l_c} p_{eq}(x) q(x) dx. \qquad (5)$$

$\delta q = q(r) - k_R$ and l_c is the contour length (8). The function $p_{eq}(x)$ describes the equilibrium end-to-end distance distribution. For one-dimensional diffusion, the time integral of the sink-sink correlation function can be evaluated analytically (9), and Eq. 4 becomes

$$\frac{1}{k_{obs}} = \frac{1}{k_R} + \frac{1}{k_R^2} \int_a^{l_c} (D(x) p_{eq}(x))^{-1} \left[\int_x^{l_c} \delta q(y) p_{eq}(y) dy \right]^2 dx. \qquad (6)$$

Equation 5 can be used to calculate k_R from simulated distributions of end-to-end distances using $q(x)$ determined by Lapidus et al. (7) and the second term of Eq. 6 can be used to calculate $1/k_{D+}$ (3).

Using this analysis, Lapidus et al. showed that for peptides having the sequence cys-(ala-gly-gln)$_j$-trp, the reaction-limited rate of loop formation in aqueous buffer became essentially length-independent for short chains, suggesting that the chain is stiff (3). Their results could be described with an end-to-end distance distribution for a wormlike chain having a persistence length of 0.6–0.7 nm. Using the one-dimensional diffusion model of Szabo, Schulten, and Schulten, the length dependence of the diffusion-limited rates could also be reproduced by treating the dynamics as diffusion on the one-dimensional potential of mean force obtained from this distribution (10). The diffusion coefficient for the chain ends that was required to fit the diffusion-influenced rates was $\sim 1.7(10^{-6})$ cm^{2}s^{-1} at a viscosity of 1 cp and 293 K.

The results for peptides with more than ~ 10 peptide bonds could be compared with those expected for random walk chains. Szabo, Schulten, and Schulten theory predicts that the diffusion limited rate of contact formation at distance a is given by

$$k_{D+} = \frac{4\pi Da}{(2\pi \langle r^2 \rangle / 3)^{3/2}} = \frac{4\pi Da}{(2\pi C_n n l^2 / 3)^{3/2}}, \qquad (7)$$

where D is the end-to-end diffusion coefficient, $\langle r^2 \rangle$ is the mean-squared end-to-end distance, n is the number of peptide bonds, l ($= 0.36$ nm) is the projection of the C_α-C_α distance on the axis of the fully extended chain, and C_n is the Flory characteristic ratio. The contact rate for a random-walk chain therefore scales as $n^{-1.5}$. The denominator of Eq. 7 describes the effective volume accessible to the chain ends, so effects that increase the average end-to-end distance would be expected to decrease the loop formation rates. For example, increasing the value of C_n decreases k_{D+}. The random walk model, however, cannot describe chains with lengths comparable to the segment length C_n. Since a wormlike chain, characterized by its persistence length, l_p, is continuous and the elastic contribution to chain deformation becomes significant for short chains (11,12), the length-dependence for short chains can be reproduced using this model. Wormlike chains also become Gaussian in the long-chain limit, so $\langle r^2 \rangle$ becomes proportional to chain length and the quenching rate scales as described by Eq. 7.

In good solvents, chains swell because the volume occupied by a given chain segment cannot be occupied by other segments of the chain (13) and these interactions are not countered by attractive interactions between chain segments. This ''excluded'' volume will decrease the diffusion-limited quenching rate for a fixed chain length. Mean-field models (14) predict that excluded volume increases the $\langle r^2 \rangle \propto n$ dependence for Gaussian chains to $\langle r^2 \rangle \propto n^{1.2}$, so the rate would be expected to scale as $n^{-1.8}$. The effect of

swelling on the diffusion-limited rate of loop closure in the long chain limit has been rather extensively studied, both by renormalization group calculations (15) and Brownian dynamics simulations (16,17). In the simulations, the cyclization time, $\tau = 1/k_{D+}$, increased with chain length as $n^{2.0\pm0.1}$ for random walk chains and as $n^{2.2\pm0.1}$ for chains with excluded volume. Recently, the effect of swelling on the diffusion-limited rate of loop closure in stiff chains has been investigated using the Wilemski-Fixman model of diffusion-controlled reactions coupled with a generalized random walk description of chain conformations (18,19). The length-dependence increased from $\tau \propto n^{2.0-2.1}$ in the absence of nonlocal interactions, to $\tau \propto n^{2.2-2.3}$ for fully swollen chains (19).

In this article, we report experiments and simulations that explore the effects of highly denaturing solvents, 6 M guanidinium chloride (GdmCl) and 8 M urea, on chain dimensions and the rate of loop formation. These have been shown to be good solvents for the model peptide tetraglycine (20). There are two major results. First, the reaction-limited rates in denaturing solvents decrease monotonically with increasing chain length, even for short peptides, and the reaction- and diffusion-limited rates exhibit a stronger length-dependence than that measured in aqueous buffer. These results are consistent with simulated distributions obtained for wormlike chains with a persistence length of the order of a single peptide bond and excluded volume. Second, we show that the loop formation rates for an 11-residue loop decrease when one of the probe residues is not the chain terminus. This is also a hallmark of chains with excluded volume (21). The results show that 6M GdmCl and 8 M urea are ''good'' solvents for our peptide, whereas aqueous buffer is very close to a θ-solvent in which the peptide can be approximately described as a wormlike chain.

METHODS

Experimental

The temperature- and viscosity-dependence of the quenching rates was measured in sucrose solutions at temperatures between 0°C and 40°C using the instrumentation and procedures described previously (3). Viscosities were measured using a Wells-Brookfield Model LVT cone-plate viscometer with a thermostatted sample chamber. The data were analyzed as described by Lapidus et al. (3). The reaction-limited rates (k_R) and diffusion-limited rates (ηk_{D+}) were obtained from the intercept and slope of plots of $1/k_{obs}$ versus the solution viscosity. To fit the data, we assume that the rates k_R, and k_{D+} can be described by

$$k_R = k_R(T_0)\exp\left(\frac{E_0(T - T_0)}{RTT_0}\right)$$

$$\eta k_{D+} = \frac{\eta(T_0)k_{D+}(T_0)}{(1 - A\eta)}\frac{T}{T_0}\exp(B(T - T_0)), \qquad (8)$$

where T is the absolute temperature, $T_0 = 273$ K, η the solution viscosity, and A, B, $k_R(T_0)$, $\eta(T_0)k_{D+}(T_0)$ and E_0 are fitting parameters. Because the viscosity-dependence at low temperatures and high sucrose concentrations is not linear, the nonlinear dependence on $1/\eta$ was incorporated in Eq. 8 to

permit accurate values for the intercepts and initial slopes to be obtained from the experimental data.

Fluorescence resonance energy transfer (FRET) experiments were carried out by measuring emission spectra of samples excited at 280 nm using a Spex spectrofluorimeter. Emission spectra were integrated from 300 to 450 nm to obtain the emitted intensity I. Transfer efficiencies were calculated as $E = 1 - I_{DA}/I_D$, where I_D is the intensity for the unquenched donor and I_{DA} is the intensity of the donor when quenched by the acceptor. Average end-to-end distances were calculated using $(R/R_0)^6 = (1 - E)/E$. The characteristic transfer distance, R_0, expressed in angstroms, is given by

$$R_0 = 0.211(\phi_D \kappa_f^2 n^{-4} J)^{1/6}, \qquad (9)$$

where ϕ_D is the quantum yield of the donor in the absence of the acceptor, κ_f^2 is a geometric factor, which has the value of 2/3 assuming that both donor and acceptor completely sample an isotropic orientational distribution during the donor lifetime, and n is the refractive index of the medium. J is a measure of the spectral overlap between donor emission F_D and acceptor absorption ε_A. In the formula above J is expressed in unit of $M^{-1}cm^{-1} (nm)^4$ and is given by

$$J = \frac{\int_o^\infty F_D(\lambda)\varepsilon_A(\lambda)\lambda^4 d\lambda}{\int_o^\infty F_D(\lambda)d\lambda}. \qquad (10)$$

Fluorescence quantum yields were calculated relative to N-acetyl-tryptophan amide (22). The overlap integral J was calculated from emission spectra measured from 290 to 450 nm and absorption spectra of the reference peptide, assuming a dansyl extinction coefficient of 4300 $M^{-1}cm^{-1}$ in water at 20°C (23). All the measurements were performed at a concentration of 5 μM (tryptophan) in 100 mM sodium phosphate buffer, pH 6.0.

Theoretical

As a first-order description of the effects of chain backbone stiffness on the equilibrium end-to-end distribution, $p_{eq}(r)$, we have utilized the wormlike chain model proposed by Porod and Kratky (24). Chain stiffness is characterized by the persistence length, l_p ($= \kappa /k_B T$), where κ is the bending rigidity. The wormlike chain model ignores both excluded volume effects resulting from backbone-backbone interactions and attractive interactions that arise from both van der Waals and hydrophobic effects. To include excluded volume effects, we have used the simple heuristic model shown schematically in Fig. 2. We assume that the volume excluded by backbone and side chains can be approximated as hard-sphere interactions between spheres of diameter d_α centered at the end of each peptide bond. The segment of the chain between spheres, which approximates the projection of each peptide bond on the contour length, has a length of 0.36 nm. To include excluded volume interactions, chains are selected in which the distances between all spheres that are not nearest neighbors exceed d_α. The chains were generated as described by Hagerman and Zimm (25). Each peptide bond, i_p, is made by adding 10 segments (of length 0.036 nm) to the chain end, and the chain is then screened by calculating the distance to the ends of all peptide bonds in the chain that are not nearest neighbors, ($j_p < i_p - 1$). If any of these distances is less than d_α, the chain is terminated and discarded. If not, chain growth continues until the maximum number of segments has been added. Zhou has used a similar procedure to model the intrinsic viscosity and Stokes radii of unfolded proteins (26).

Sample distributions of end-to-end distances for an 11-residue peptide (10 segments) obtained with a series of increasing values of d_α are shown in Fig. 3. As the excluded volume increases, a larger fraction of the more compact chains violates the constraint, and the peak of the distance distribution moves to larger distances. The results show that excluded volume decreases the probability of short distances relative to that for the ideal wormlike chain. This results in an increase in the apparent persistence length, as shown in the inset to Fig. 3 and a decrease in k_R. One means of characterizing these distributions is to utilize the Domb-Gillis-Wilmers function, $W(r,n)$, written as
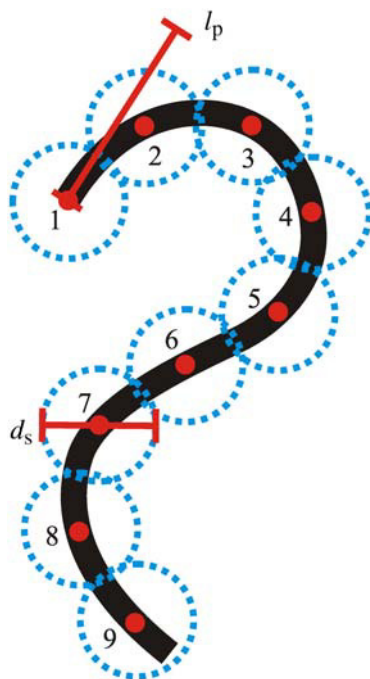
FIGURE 2 Schematic of a wormlike chain with excluded volume. The peptide backbone is assumed to have a uniform rigidity, κ, corresponding to a persistence length, $l_p = \kappa/k_B T$. The chain is assumed to have 10 segments per peptide bond (0.36 nm). The excluded volume model assumes that a hard sphere of diameter d_α is present at the end of each peptide bond and conformations in which two bond termini that are not nearest neighbors are closer than d_α are excluded from the simulated ensemble. Since tryptophan-cysteine distances are considered explicitly in calculating the rates, configurations for which the chain distance between these two residues is less than d_α are included.

$$W(r, n) = C_n r^l \exp\left[-(r/\sigma_n)^t\right] \qquad (11)$$

This function, which provides an empirical expression for the end-to-end distribution in the presence of excluded volume (27), is frequently used to represent empirical results on swollen polymers. It is written in terms of the adjustable parameters, l and t, with

$$
\begin{aligned}
C_n^{-1} &= (\sigma_n^{l+1}/t)\Gamma[(l+1)/t] \\
\sigma_n^2 &= \langle r^2 \rangle \Gamma[(l+1)/t]/\Gamma[(l+3)/t],
\end{aligned}
\qquad (12)
$$

where n is the number of chain elements and Γ is the gamma function. The mean squared end-to-end distance $\langle r^2 \rangle$ is given by $\langle r^2 \rangle = A\, n^{2\nu}$, where $\nu = 1 - 1/t$. In "good" solvents, the dependence of $\langle r^2 \rangle$ on chain length is steeper than for an ideal chain, with 2ν approaching 1.18 when the chain is fully swollen (28). We note that the end-to-end distributions for the 11- and 20-residue peptides obtained from the Langevin dynamics simulations reported by Lapidus et al. (3) are well-fitted using this expression (Eq. 12) with $l = 2$ and $t = 4$.

Fits using this function are shown in Fig. 3 and the fitting parameters are summarized in Table 1. Although the fits are reasonably accurate near the most probable distance, they differ significantly at short end-to-end distances where accuracy is most critical when calculating k_R. Consequently, spline fits to the simulated distributions were routinely used to calculate values of k_R from the simulated distributions.
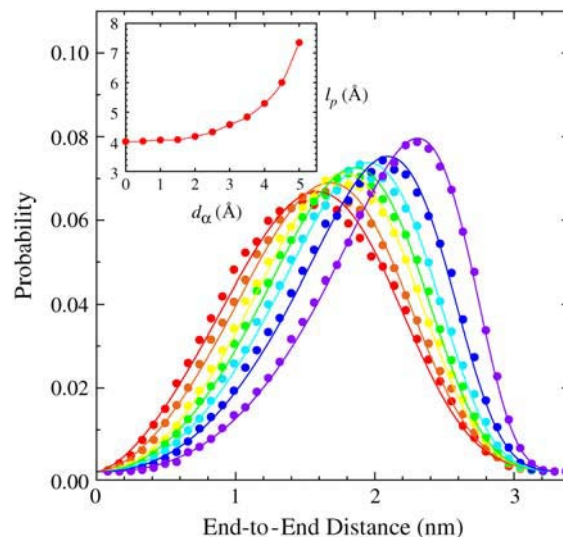

FIGURE 3 Effect of excluded volume on end-to-end distributions calculated for an 11-residue peptide. The results of 10^5 trials are shown for no excluded volume (*black*) and excluded distances of 0.3 nm (*blue*), 0.4 nm (*light blue*), 0.5 nm (*green*), 0.55 nm (*magenta*), and 0.6 nm (*red*). The fits shown are those obtained using the Domb-Gillis-Wilmers function (Eqs. 11 and 12). The fit parameters are shown in Table 1. (*Inset*) Calculated values of l_p obtained from the simulated distance distributions as the average projection of the end-to-end vector on the first chain segment.

RESULTS

Qualitative description of the data

Fig. 4 shows the results from representative experiments in which the optical density after nanosecond excitation of the tryptophan for the peptide is shown as a function of time. Data from a set of peptides with sequences C(AGQ)$_j$W of different lengths are shown in Fig. 4, *top*, and data for peptide C(AGQ)$_3$W (*cxw*, Table 2) at different solution viscosities are shown in Fig. 4, *bottom*. The decay curves were fitted using two exponential relaxations. The faster process is the decay of the tryptophan triplet state, whereas the slower process results from formation of another photoproduct, a tryptophan radical (29). The triplet lifetimes for three peptide lengths are plotted as a function of solution

TABLE 1   Fits to simulated distance distributions for a chain with 10 peptide bonds

d_α (nm)	l	t	σ_n	fss*
0	1.51	7.28	6.99	0.0014
0.25	1.71	7.06	6.94	0.0014
0.30	1.80	6.97	6.91	0.0015
0.35	1.91	7.14	6.92	0.0012
0.40	2.01	7.35	6.97	0.0014
0.45	2.10	7.92	7.09	0.0011
0.50	2.25	8.95	7.28	0.0009
0.55	2.56	11.1	7.60	0.0004
0.60	3.25	15.4	8.00	0.0002

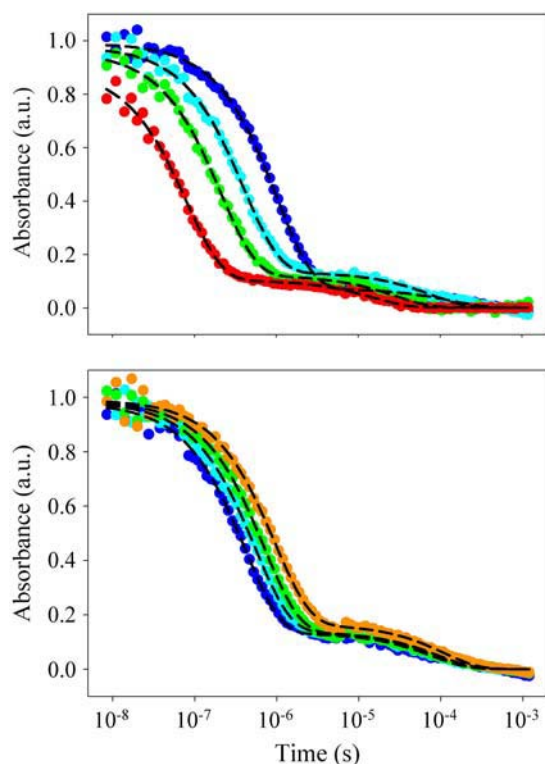*Sum of squared residuals from fit to Eqs. 11 and 12.

FIGURE 4 Decay of the triplet state of tryptophan. (*Top*) Absorbance decays measured for peptides $C(AGQ)_1W$ (*red*), $C(AGQ)_2W$ (*green*), $C(AGQ)_3W$ (*cyan*), and $C(AGQ)_6W$ (*blue*) at 20°C in the absence of sucrose. (*Bottom*) The absorbance decays at 20°C for the peptide $C(AGQ)_3W$ (*cxw*) in solutions containing 0 M (*blue*), 0.5 M (*cyan*), 0.73 M (*green*), and 0.92 M (*orange*) sucrose. The broken lines are the fits obtained using two exponential relaxations. The measured transient absorbance for all samples was 6 mOD ($\pm$ 2 mOD). To compare the decays, each absorbance change has been normalized. Samples were prepared at a concentration of 50 mM ($\pm$10 mM) in 6M GdmCl solution saturated with N_2O.

TABLE 2 Peptide sequences

Peptide name	Sequence
cxw	cys-(ala-gly-gln)$_3$-trp
qcxw	gln-cys-(ala-gly-gln)$_3$-trp
xcxw	(ala-gly-gln)$_3$-cys-(ala-gly-gln)$_3$-trp
dxw	dansyl-(ala-gly-gln)$_3$-trp
qxw	gln-(ala-gly-gln)$_3$-trp
dpw	dansyl-(pro)$_6$-trp

top, and the values in the absence of denaturant are shown in Fig. 6, *bottom*. The values of k_R are determined by the average of the quenching rate over the end-to-end distance distribution (Eq. 5). For the shortest chains, the values of k_R and those of ηk_{D+} are very similar under all solution conditions. As the chain length increases, however, the rates in the denaturing solvents become progressively slower. As predicted by models (17) and theoretical calculations (19), the length dependence of the diffusion-limited rate is higher in the presence ($\eta k_{D+} \propto n^{-2.0}$) than in the absence of denaturant ($\eta k_{D+} \propto n^{-1.7}$). The dependence of k_R on chain length for the longest chains also increases, albeit slightly, from $k_R \propto n^{-1.55(\pm 0.05)}$ to $k_R \propto n^{-1.65(\pm 0.05)}$ in both 6 M GdmCl and 8 M urea.

The decreases in the reaction-limited and diffusion rates and their increased dependence on chain length upon the addition of denaturants suggest that the chains are swelling from excluded volume effects. These effects were also studied by a different kind of experiment using the peptides *qcxw* and *xcxw* (Table 2) in which either one residue or nine residues are added to the amino-terminus to lengthen the 11-residue peptide. Adding residues to the amino-terminus reduces access to the cysteine, which is now an interior residue, through excluded volume effects (21). The results of these experiments are shown in Fig. 7, where it is seen that the addition of a single glutamine residue reduces the rate by a factor of 1.5, not much smaller than the 1.7-fold reduction observed with the nine-residue tail for the peptide *xcxw*.

To confirm that the chain swells from excluded volume effects on the addition of denaturant, we also performed FRET experiments to determine changes in the end-to-end distance distribution by adding dansyl to the amino-terminus of the peptide. The peptide sequences used for these measurements are given in Table 2. The 11-residue peptide *dxw* was chosen because its average end-to-end distance, estimated as ~2.0 nm, is close to the R_0 for the tryptophan-dansyl pair. As a control, we used the shorter proline peptide *dpw*. Fluorescence emission spectra are shown in Fig. 8. Since the emission spectra at all GdmCl concentrations can be superimposed by scaling, the environment of the tryptophan appears to be unaffected by either solvent or peptide sequence. The quantum yield of both peptides increases significantly with increasing GdmCl concentration, but the change in *dxw* is significantly greater than that for *dpw*. The effect of GdmCl presumably results from the fact that

viscosity in Fig. 5. The fitted rates for all peptide lengths appear to fall on straight lines at temperatures above 290 K, but the values at lower temperatures exhibit distinctive negative curvature. Since the curvature increases with increasing peptide length, we hypothesize that it results from intrachain interactions that are largest at low temperature and high sucrose concentrations. If these interactions act to decrease the dimensions of chain, then the measured rates would not decrease linearly as η^{-1}. Since we are interested in obtaining accurate values for the intercepts and for initial slopes that scale as η^{-1} (see Qiu and Hagen for a discussion of this scaling (30)), we have chosen to fit the results using a quadratic function of viscosity (see Methods). The diffusion-limited rates obtained from these fits are therefore expected to be relevant in the absence of sucrose. The fitted values of $k_R(T_0)$, $\eta(T_0)k_{D+}(T_0)$, E_0, and B (Eq. 8) for all of the peptides studied are given in Table 3.

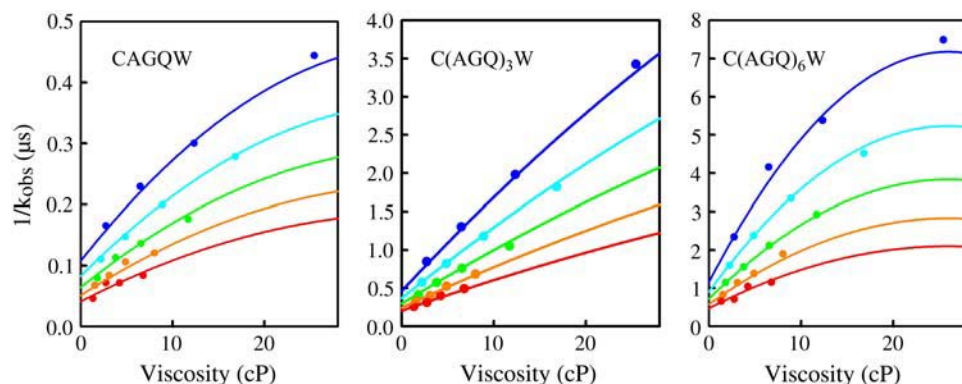The diffusion-limited (ηk_{D+}) and reaction-limited (k_R) rates at 20 C in 6 M GdmCl and 8 M urea are shown in Fig. 6,

FIGURE 5 Temperature-and viscosity-dependence of quenching rates for cys-(ala-gly-gln)$_j$-trp. The measured triplet lifetimes for the (*left panel*) $j = 1$, (*middle panel*) $j = 3$, and (*right panel*) $j = 6$ peptides are plotted at 0 C (*blue*), 10 C (*cyan*), 20 C (*green*), 30 C (*orange*), and 40 C (*red*) as a function of viscosity and fitted to Eq. 8. Values for the parameters $k_R(T_0)$ (s^{-1}), $\eta(T_0)k_{D+}(T_0)$, E_0, A, and B (Eq. 8) were obtained by fitting the data for each peptide length. The fitted values are given in Table 3.

the primary quenching mechanism of the tryptophan singlet excited state is electron transfer to water, which is less efficient in the mixed solvents. FRET-averaged distances can be obtained from these results in two ways. The first is to determine values of R_0 at each set of conditions by measuring the values of ϕ_D, n, and J (Eqs. 9 and 10). The results, presented in Table 4, show that R_0 decreases at higher temperature, primarily as a result of the decrease in ϕ_D. Using these values, the end-to-end distances, $\langle r^6 \rangle^{1/6}$, calculated for the rigid peptide *dpw*, change by only ~1%. Note, however, that the FRET-determined end-to-end distance for *dpw* is significantly shorter than that estimated from the polyproline II structure (31), which ranges from 2.1 to 2.7 nm, depending on the conformation of the tryptophan residue. As observed in the loop formation experiments, the end-to-end distances calculated for the random peptide *dxw*

increase significantly (by ~15%) in 6M GdmCl at both 0°C and 60°C, confirming that the chain swells in denaturing solvents.

Similar results are obtained using a purely empirical approach, in which peptide *dpw* is used as a standard, with a length that is assumed to be independent of temperature and GdmCl concentration. If the measured transfer efficiencies for *dpw* is used to determine the dependence of R_0 on solution conditions, the change in the end-to-end distance, $\langle r^6 \rangle^{1/6}$, of *dxw* is calculated to be ~10%, in good agreement with the results in Table 4. The relative lengths obtained using both approaches are similar, because there is very little change in the end-to-end distance of *dpw* calculated using the spectroscopically determined R_0 (Table 4). The principal difference is that the lengths obtained using *dpw* as a standard are significantly longer.

TABLE 3   Parameters obtained from fits to the temperature-and viscosity-dependence of quenching rates

	Water data			
Peptide	$k_R(T_0)$ (s^{-1})*	$\eta(T_0)k_{D+}(T_0)$ (cp s^{-1})	E_0 (kcal mol^{-1})	A
C(AGQ)$_1$W	1.64 (10^7)	9.4 (10^7)	5.12	0.0149
CA(AGQ)$_1$W	1.48 (10^7)	1.27 (10^8)	3.29	0.0322
CQ(AGQ)$_1$W	1.73 (10^7)	7.51 (10^7)	1.83	0.0391
C(AGQ)$_2$W	1.08 (10^7)	4.02 (10^7)	3.61	0.0272
C(AGQ)$_3$W	7.4 (10^6)	2.37 (10^7)	3.23	0.0238
C(AGQ)$_4$W	5.2 (10^6)	1.95 (10^7)	3.31	0.0134
C(AGQ)$_6$W	2.66 (10^6)	1.47 (10^7)	3.60	0.0043
C(AGQ)$_9$W	1.51 (10^6)	1.09 (10^7)	1.42	0.0368
	GdmCl data			
Peptide	$k_R(T_0)$ (s^{-1})*	$\eta(T_0)k_{D+}(T_0)$ (cp s^{-1})	E_0 (kcal mol^{-1})	A
C(AGQ)$_1$W	1.55 (10^7)	8.3 (10^7)	4.09	0.0189
CA(AGQ)$_1$W	1.21 (10^7)	5.3 (10^7)	2.70	0.0259
CQ(AGQ)$_1$W	1.28 (10^7)	4.5 (10^7)	3.35	0.0239
C(AGQ)$_2$W	6.9 (10^6)	2.31 (10^7)	4.06	0.0262
C(AGQ)$_3$W	3.4 (10^6)	1.36 (10^7)	3.48	0.0238
C(AGQ)$_4$W	2.9 (10^6)	0.76 (10^7)	1.30	0.0245
C(AGQ)$_6$W	1.40 (10^6)	0.42 (10^7)	3.83	0.0293
C(AGQ)$_9$W	0.79 (10^6)	0.19 (10^7)	5.78	0.0151

*$T_0 = 273$ K.

Dependence on temperature

The results in Fig. 5 also show that both the reaction and diffusion-limited rates exhibit significant temperature dependence. Both the intercepts ($1/k_R$) and the slopes ($1/\eta k_{D+}$) of the fits to the viscosity-dependence increase significantly at low temperatures. As expected from Eq. 5, the temperature dependence of k_R (Table 3) is primarily determined by that of the quenching rate, $q(x)$, with an apparent activation energy of ~3 kcal/mol, the activation energy for quenching of N-acetyl-tryptophan amide by free cysteine. The variation in the fitted activation energies is more than ± 1 kcal/mol, so it is difficult to discern any variation with chain length or solution conditions from these results, suggesting that there is little or no temperature dependence to the distribution function $p_{eq}(x)$ (Eq. 5). The temperature-dependence of the diffusion-limited rates, ηk_{D+}, shown in Fig. 9, is somewhat greater than that of k_R. In both 6 M GdmCl and 8 M urea, the rates for all peptide lengths exhibit very similar temperature-dependence, with an apparent activation energy of −5 kcal/mol. In water, however (data not shown), the rates for the shortest peptides are significantly more temperature dependent than the longest, resulting in a decrease in the

TABLE 4 Resonance energy transfer results

Peptide	T (C)	[GdmCl] (M)	E	n	ϕ_D	$J \times 10^{13} (M^{-1} cm^{-1} (nm)^4)$	R_0 (Å)	$\langle R^2 \rangle^{1/2}$ (Å)
dxw	20	0	0.794	1.3345	0.08	3.404	19.30	14.6
	20	6	0.693	1.4360	0.12	3.498	19.55	17.3
	60	0	0.706	1.3303	0.04	3.676	17.07	14.8
	60	6	0.615	1.4298	0.06	3.644	17.59	17.3
dpw	20	0	0.701*	1.3345	0.14	3.757	21.38	18.5
	20	6	0.621*	1.4360	0.13	3.436	19.89	18.3

length-dependence at low temperature, suggesting that the longer chains may be becoming more compact at low temperature.

Theoretical modeling

To examine the results on the reaction- and diffusion-limited rates more quantitatively, we need a model to describe the end-to-end distance distribution, $p_{eq}(r)$ (Eqs. 4–6). The model must incorporate chain stiffness to describe the turnover in the rates for the shortest chains in the absence of denaturant as well as excluded volume interactions to describe the changes in slope observed in denaturing solvents. Accordingly, we have introduced excluded volume into the wormlike chain model used previously (3) by excluding configurations in which the ends of nonadjacent chain segments lie within an excluded distance, d_α. The repulsive interactions modify the distribution by selectively removing conformations with shorter end-to-end distances and hence increasing the effective persistence length (see Fig. 3). Since the cumulative effect is larger for longer chains, the effective persistence length also becomes length dependent. We shall refer to this model as the WCX model.

To describe the data, we need to find approximate values of d_α and l_p which are consistent with the experimental results under all sets of solution conditions. This problem was initially approached by assuming from the measured length dependence in the absence of denaturant, which approaches the $k_R \propto n^{-3/2}$ dependence expected for Gaussian chains, that the excluded volume is almost perfectly compensated by weak attractive interactions and that water approximates a θ-solvent. In the classic picture described by Flory, the excluded volume of the chain must be compensated by attractive interactions in a solvent in which the chain behaves as a Gaussian chain. If this were true, then the excluded volume could be estimated as that required to reduce the values of k_R for longer chain lengths to those measured in 6 M GdmCl and 8 M urea. Initially, we attempted to describe the rates in denaturing solvents using the WCX model with the persistence length previously determined from a fit to the data in aqueous buffer (0.65 nm) (3) and found that a sphere diameter of $d_\alpha = 0.44$ nm could reproduce the measured values of k_R for long chains in 6 M GdmCl and 8 M urea. This approach, however, predicted significantly more flattening of the rates for short chains than

is observed for the measured values. To match the measured rates for all peptide lengths, distributions were simulated with progressively shorter persistence lengths. The best approximation of the data was obtained using $l_p = 0.40$ nm and $d_\alpha = 0.40$ nm. The calculated rates are shown in Fig. 6, *top*. It should be pointed out that the rates for the model are selected from those calculated from a library of numerically simulated distributions, $p_{eq}(x)$, using Eqs. 5 and 6, as those that best describe the measured rates, so the differences between the observed and calculated rates have not been numerically minimized to optimize the values of l_p and d_α.

We have used the same approach to match the data on reaction-limited rates for water shown in Fig. 6, *bottom*. Most of these rates have been redetermined in this study by the analysis of new experimental data. The slope for long peptides in these data is slightly greater than $k_R \propto n^{-1.5}$ predicted for a chain without excluded volume. In addition, the flattening for the shortest peptides is somewhat less pronounced than in the data of Lapidus et al. (3). The best match to the measured data is obtained with a persistence length $l_p = 0.55$ nm and a sphere diameter $d_\alpha = 0.20$ nm. The short persistence length produces flattening of the reaction-limited rates, not the turnover predicted from considerations of loop formation probability that assumed that polypeptide chains were significantly stiffer (11,12). Using these values of l_p and d_α, the diffusion limited rates calculated from Eq. 6 in the presence and absence of denaturants can also be reasonably-well fit with diffusion coefficients of $D/\eta = 0.8$–0.9 (10^{-6}) cm^2 s^{-1}cp^{-1} and $D/\eta = 1.4$–1.6 (10^{-6}) cm^2 s^{-1}cp^{-1}, respectively. The latter is very close to the value of 1.7 (10^{-6}) cm^2 s^{-1}cp^{-1} obtained by Lapidus et al. (3).

The sphere diameter, d_α, can be independently estimated from the change in the reaction-limited rate in denaturing solvents measured when additional residues are added at either end of the chain. The results in Fig. 7 are compared with rates calculated as a function of the length of the "tail" for $d_\alpha = 0.38$ nm and $d_\alpha = 0.40$ nm. The ratio of the rates increases with d_α and is comparable to the observed ratio for $d_\alpha \approx 0.38$ nm. The experimentally measured ratio of rates for tail lengths of 0 and 1 ($k_{qcxw}/k_{cxw} = 0.68$) is reproduced using $d_\alpha = 0.3$ nm, whereas the experimental rate for peptide *xcxw* ($k_{xcxw}/k_{cxw} = 0.62$) is best reproduced using $d_\alpha = 0.37$ nm. From these results, we conclude that values of d_α between 0.35 nm and 0.4 nm can approximately reproduce the experimental results.
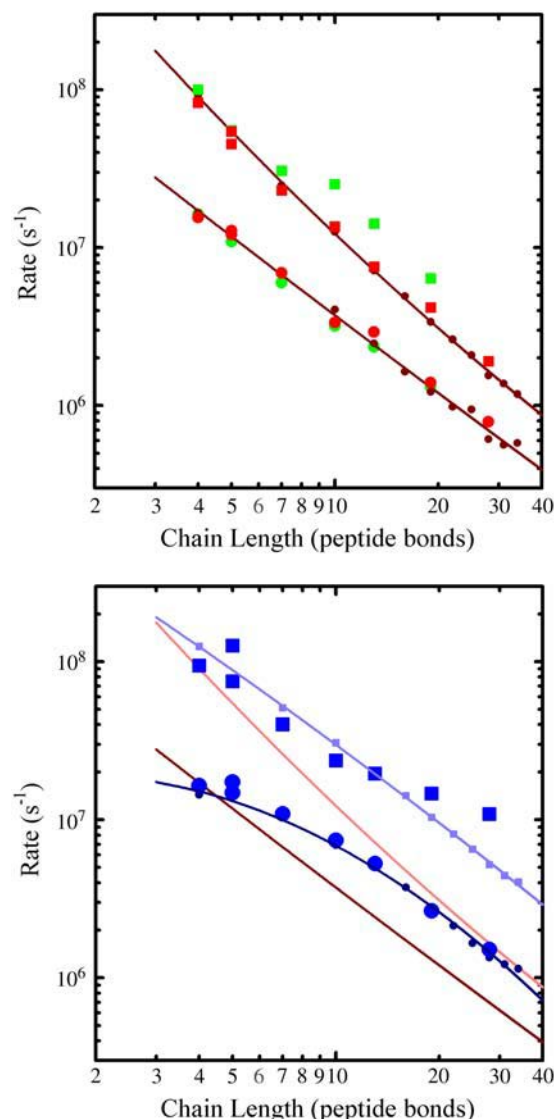
FIGURE 7 Effect of tails on rate of loop formation. The large red points are the measured rates for peptides C(AGQ)$_3$W, QC(AGQ)$_3$W, and (AGQ)$_3$C(AGQ)$_3$W scaled relative to the measured rate for C(AGQ)$_3$W. The simulated rates for $l_p = 0.4$ nm and $d_\alpha = 0.38$ nm (*magenta*) and $d_\alpha = 0.4$ nm (*green*) are shown as the small dots. The magenta and green lines were obtained by averaging the rates calculated for all tail lengths >0. The blue points are the relative rates calculated from a three-dimensional lattice model by Chan and Dill (35).

FIGURE 6 Length dependence of quenching rates for cys-(ala-gly-gln)$_j$-trp peptides at 20°C. (*Top*) Reaction- and diffusion-limited rates in 6M GdmCl and 8 M urea. The red symbols are the values of k_R (*red circles*) and ηk_{D+} (*red squares*) obtained from the analysis of the temperature- and viscosity-dependence of the measured rates in 6M GdmCl (Table 3). The green symbols are the values of k_R (*green circles*) and ηk_{D+} (*green squares*) measured in 8 M urea. The dark red symbols are the values of k_R (*small circles*) and ηk_{D+} (*squares*) calculated from simulations using $l_p = 0.4$ nm and $d_\alpha = 0.4$ nm and the lines are polynomial fits to the calculated rates. The dark red lines are polynomial fits to the reaction- and diffusion-limited rates calculated from the simulations: $\log(k_R) = 18.95 - 1.65 \log(n)$; $\log(\eta k_{D+}) = 21.04 - 2.025 \log(n)$, where n is the chain length (peptide bonds). (*Bottom*) Reaction- and diffusion-limited rates in aqueous buffer. The large blue symbols are the values of k_R (*circles*) and ηk_{D+} (*squares*) obtained from the analysis of the temperature- and viscosity-dependence of the measured rates in 6M GdmCl (Table 3). The small blue symbols are the values of k_R (*dots*) and ηk_{D+} (*squares*) calculated from simulations using $l_p = 0.55$ nm and $d_\alpha = 0.2$ nm. The light and dark blue lines are polynomial fits to the reaction and diffusion limited rates calculated from the simulations: $\log(k_R) = 17.5 - 0.24 \log(n) - 0.23 (\log(n))^2$; $\log(\eta k_{D+}) = 21.17 - 1.725 \log(n)$. The dark and light red lines are the fits to the calculated values of k_R and ηk_{D+}, respectively, described in the top panel.
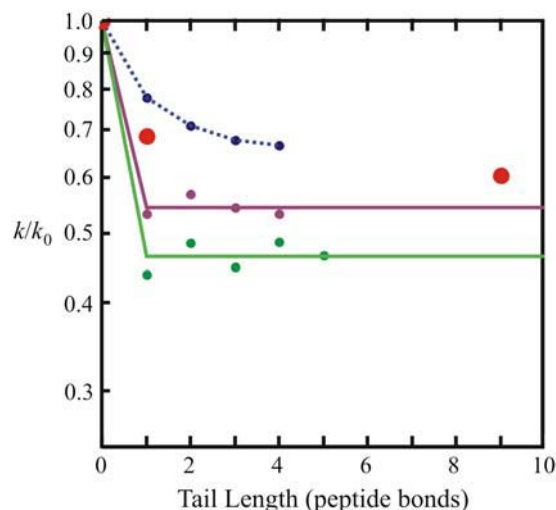
How well do the calculated distributions compare with the results of the FRET experiments (Table 4)? The effect of d_α on the end-to-end distance distributions for the 11-residue peptide used in the FRET experiments is shown in Fig. 3. The value of $\langle r \rangle$ calculated from these distributions increases by ~8% (from 1.88 for $d_\alpha = 0$ to 2.03 nm for $d_\alpha = 0.45$ nm). The swelling predicted by the model is thus in reasonable agreement with the results of the FRET experiments. We note, however, that the calculated distances are significantly larger than those in Table 4. One interpretation of this result is to note that the FRET-determined distances for peptide *dpw* are also significantly smaller than the end-to-end distance of this peptide estimated from its ideal structure, an effect that could result from the dimensions of the probes, from departures from the dimensions calculated by assuming that the solution structure is identical to the fiber structure (32), or from hydrophobic interactions between dansyl and tryptophan which perturb the end-to-end distance distribution of *dxw*. If FRET-determined distances are systematically short, then there is reasonable consistency between the simulated distributions and the results of the FRET experiments. In the worst-case, that is if Forster's equation (Eq. 9) is accurate and *dxw* is a reasonably accurate model for *cxw*, one must conclude either that the wormlike chain provides a rather poor description of the end-to-end distance distribution for our peptides or that the FRET probes are significantly biasing the distance distribution by favoring shorter end-to-end distances. The FRET experiments can then only be viewed as qualitative support for the swelling observed in the loop formation experiments.
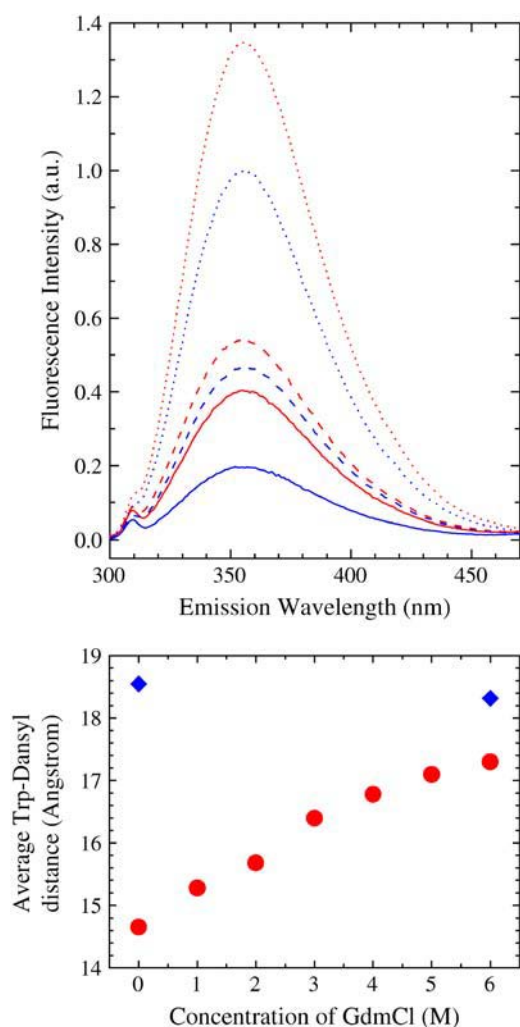
FIGURE 8 Measurement of average end-to-end distance by FRET. (*Top*) The emission spectra for dansyl-(ala-gly-gln)$_3$-trp (*dxw*) in aqueous buffer (*blue*) and 6 M GdmCl (*red*) are shown as solid lines. Spectra of the control peptide gln-(ala-gly-gln)$_3$-trp (*qxw*) are shown as dotted lines, and spectra of dansyl-(pro)$_6$-trp (*dpw*) are shown as dashed lines. All samples were excited at 280 nm. (*Bottom*) Dependence of end-to-end distance on GdmCl concentration. The Forster-averaged distance for *dxw*, calculated as in Table 4, is shown as the red points. The blue points are the values reported in Table 4 for peptide *dpw*.

DISCUSSION

Reaction-limited rates and chain conformation

Since the measured quenching rates in the absence of added sucrose are close to reaction limited, the experiments presented here show clearly that high denaturant concentrations (6 M GdmCl or 8 M urea) lower the reaction limited rates (k_R) compared to zero denaturant. A more surprising result is the absence of any curvature for the shortest peptides, indicating a significant decrease in chain stiffness in the presence of denaturants. Assuming no change in the distance dependence of the quenching rate ($q(x)$ in Eq. 5), the decrease in k_R can be explained by increased excluded volume effects in the ''good'' solvents that swell the chain

and decrease the probability of short end-to-end distances. FRET experiments on peptides in which dansyl has been added as an acceptor indicate that the end-to-end distance does, indeed, increase in the presence of denaturants, but there is some uncertainty as to the exact magnitude of this increase because of approximations in the FRET analysis and the possibility of changes in the end-to-end distance distribution due to interactions introduced by the hydrophobic dansyl group. Excluded volume effects are also predicted by simple polymer models to increase in the slope of the length dependence (14), and a slight increase clearly occurs in our data; the dependence of k_R on chain length for the longest chains increases from $k_R \propto n^{-1.55\ (\pm 0.05)}$ observed in aqueous buffer to $k_R \propto n^{-1.7\ (\pm 0.05)}$ in both 6 M GdmCl and 8 M urea.

To quantitatively explain the data, we employed a wormlike chain model used previously (3) with the addition of excluded volume. End-to-end distributions were generated by eliminating configurations in which the ends of nonadjacent chain segments lie within an excluded distance, d_α. As shown from the simulations in Fig. 3, this method effectively increases the persistence length by selectively removing configurations with shorter end-to-end distances from the distribution. The best fit to the data was obtained with a persistence length of $l_p = 0.40$ nm and $d_\alpha = 0.40$ nm in the presence of denaturant and $l_p = 0.55$ nm and $d_\alpha = 0.20$ nm in the absence of denaturant. An independent measure of $d_\alpha \approx 0.35$ nm was obtained using the same model to fit the decrease in k_R in denaturing solvents due to the addition of a ''tail'' of residues (Fig. 7). The effect of lengthening the chain on the loop probability is well-known and has been estimated from analytical theory (33) as well as from lattice models (34–36).

Both experiment and simulation show that k_R decreases significantly when even a single residue extends the chain and there is little or no additional effect by further lengthening the ''tail''. Although this result appears surprising, it is actually quite reasonable. The residue immediately adjacent to the cysteine excludes a large fraction of the volume accessible to the other end of the peptide and, since additional residues are almost always significantly farther away than d_α, they are relatively ineffective at changing the quenching rate. A decrease in the loop probability for interior loops was also found by Chan and Dill from exhaustive enumeration of lattice models (21). Although most of the decrease was found to accompany the addition of a single residue, the asymptotic value of the reduction factor was reached for somewhat longer tail lengths (2–3 residues). The precise effect of added residues must depend on the detailed stereochemistry of the cysteine, tryptophan, and added residues, so a more precise comparison will require both additional experiments in which the tail residues are varied and molecular dynamics calculations.

One might ask whether our description of a disordered polypeptide as a wormlike chain with excluded volume has

relevance to other sequences and to the chemically denatured states of proteins. In Fig. 10 we show the values of $\langle r^2 \rangle$ obtained from our simulations of the data in denaturing solvents and those calculated from the SAXS data on a number of denatured proteins summarized by Millett and co-workers (37,38). A linear extrapolation of the values of $\langle r^2 \rangle$ that describe our model peptides provides an excellent representation of the experimental values obtained for proteins unfolded in denaturants. This result suggests that these chains can also be described as wormlike chains with l_p ~0.4 nm. Using a larger persistence length ($l_p = 0.6$ nm) increases the calculated values of $\langle r^2 \rangle$ by a factor of ~1.5, significantly overestimating the SAXS results. Simulations by others, in which more complete details of the unfolded chains, together with long-range excluded volume are included, also agree well with measured values of hydrodynamic radii and R_g (26,39). For short chains of <60 amino acids, where distributions can be compared, the distributions calculated by Goldenberg (39) are significantly sharper than those calculated with the wormlike chain model, but have similar mean values.

We also find that the flexibility of chains in denaturing solvents is greater than that of the same chains in aqueous solution. This result can be rationalized with insight obtained in a recent study in which the effect of GdmCl and urea on the diffusion-limited rate of loop formation in poly(glycine-serine) peptides of different lengths (40), which showed that the dependence of the rates on denaturant concentration can be fitted using the weak binding model. In this model, proposed by Schellman (41–43), Jencks (20), and Tanford (44–46), denaturants bind weakly to the peptide backbone and the binding sites become saturated at high denaturant concentrations. The effective binding constants derived from this analysis (0.62 M^{-1} for GdmCl and 0.26 M^{-1} for urea) are similar to those obtained from measurements of the solubility of a tetraglycine peptide (20). The increased chain flexibility, which might result from changes in the distribution of allowed conformers in ϕ,ψ space in the presence of bound GdmCl or urea (47), has important implications for protein unfolding, since it suggests that, in addition to the mass action effect of denaturant binding, the entropy of the unfolded chain of a protein is higher in denaturing solvents than in aqueous solvents at high temperature. For a random coil chain, the backbone conformational entropy is estimated to be ~4 cal/(mol K residue) (48–50). An approximate estimate of the increase in entropy can be obtained for long, freely jointed chains, where the contribution from chain bending can be estimated as the rotational entropy of the n independent segments. Using our values of the segment lengths ($2l_p$), this contribution increases from ~1 cal/(mol K residue) in water to ~1.4 cal/(mol K residue) under denaturing conditions (since our peptide has a high glycine content, these values may be somewhat larger than for most protein sequences (51,52)). Although these values are significantly smaller than the total backbone entropy because
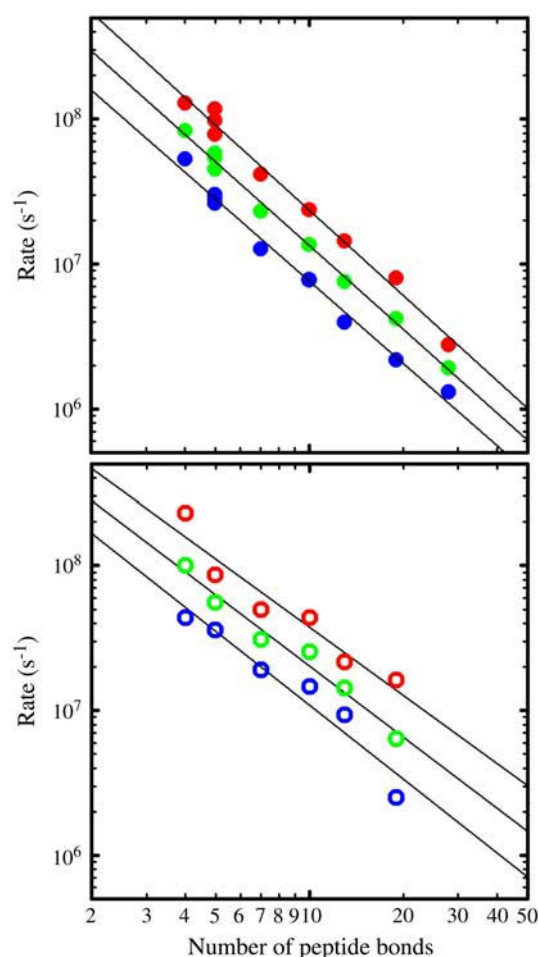

FIGURE 9 Temperature dependence of diffusion-limited rates in (*top*) 6 M GdmCl and (*bottom*) 8 M urea. The symbols are the values of ηk_{D+} (*solid circles*, 6 M GdmCl; *open circles*, 8 M urea) at temperatures of 40 C (*red*), 20 C (*green*), and 0 C (*blue*) obtained from the analysis of the temperature- and viscosity-dependence of the measured rates (Table 3). The lines are linear regression fits to guide the eye. The apparent activation energies average 4.8 (± 0.4) kcal/mol in 6 M GdmCl and 5.7 (± 0.7) kcal/mol in 8 M urea.

degrees of freedom that are effectively rotations about the chain axis are not included, the estimated 0.4 cal/(mol K residue) increase in chain entropy would contribute to the destabilization of folded structure by denaturants.

Diffusion limited rates and chain diffusion

As observed for k_R, the diffusion-limited rates, ηk_{D+}, for the shortest chains are very similar under all solution conditions. The length dependence observed in aqueous buffer can be approximated as $\eta k_{D+} \propto n^{-1.7}$, and is significantly weaker than that found in denaturing solvents, $\eta k_{D+} \propto n^{-2.0}$. The increase in slope is qualitatively consistent with theoretical models, although the slope in denaturing solvents is slightly smaller than the value of $\eta k_{D+} \propto n^{-2.2}$ predicted for fully

swollen chains (17,19). The measured values of ηk_{D+} also permit us to estimate the diffusion coefficient for the ends of the peptide chain, which is an important parameter in describing more complex properties of polypeptides. It has, for example, been recently used, in conjunction with single molecule experiments, to place an upper bound on the free energy barrier for the folding of a small protein (53). It also plays a role in determining rates in diffusion-collision models for protein folding kinetics (54–57). From fitting the diffusion limited rates, we find that the value of the diffusion coefficient is smaller in the presence of denaturants, where $D/\eta = 0.8$–0.9 (10^{-6}) cm^2 s^{-1}cp^{-1}, than in aqueous buffer, where $D/\eta = 1.4$–1.6 (10^{-6}) cm^2 s^{-1}cp^{-1} (note that values of D, which are 2–4 times smaller than our fitted value, have been reported for longer polypeptide chains (58–60), where chain stiffness is significantly less important, but interresidue interactions might contribute to slowing diffusion). Binding of denaturants, which is responsible for the increase in $\langle r^2 \rangle$ and the decrease in the reaction-limited rates for long chains, decreases the diffusion coefficient for the chain ends.

Some insight as to the possible origin of this result can be obtained from examination of the dependence of the loop formation rates on temperature. As discussed above, the temperature-dependence of k_R suggests that $p_{eq}(x)$ exhibits no significant temperature dependence, so the temperature dependence of ηk_{D+} (Fig. 9) must arise primarily from D/η, which increases with temperature from 0.4–0.5(10^{-6}) cm^2 s^{-1}cp^{-1} at 0 C to 1.4–1.5 (10^{-6}) cm^2 s^{-1}cp^{-1} at 40 C in 6 M GdmCl. Very similar results are obtained in 8 M urea. Activated diffusion has been previously reported for diffusion-limited contact formation in peptides (51) with viscosity-corrected activation energies of 2.5–4 kcal/mol for peptides that did not contain proline (51). Qiu and Hagen have also reported a viscosity-corrected activation energy of ~3 kcal/mol for the folding of the Trp cage (30). The temperature dependence observed for our sequence is thus somewhat larger than that observed in these studies.

A temperature-dependent D/η suggests that the motion of the chain ends must involve motion over local barriers that do not arise from solvent friction. The most obvious explanation is that diffusion of the peptide ends requires backbone motions that involve changes in the (ϕ,ψ) dihedral angles that encounter energetic barriers, which are observed in Ramachandran plots (61,62). The 2–4 kcal/mol barriers for helix propagation in water observed in the simulations of Young and Brooks are comparable to the observed activation energy for chain diffusion. The relaxation time for these rotations, estimated to be ~100 ps in aqueous solution (63), is significantly longer than that for solvent damping. The ''internal friction'' resulting from these barriers is thus significantly greater than the solvent friction at room temperature, and slows diffusion relative to that of free amino acids. In the presence of GdmCl or urea, denaturant binding would be expected to both increase the effective volume of the polypeptide chain (47) and to increase the
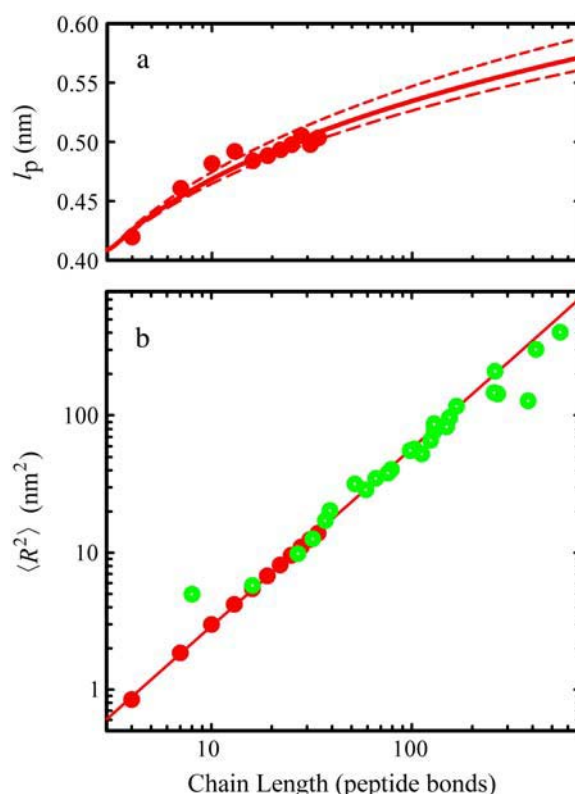

FIGURE 10 Comparison of calculated values of $\langle r^2 \rangle$, with SAXS results for denatured proteins. (*a*) Effective persistence lengths from simulations. The red points are the values of l_p obtained from the simulations as the averaged projection of the end-to-end vector on the first chain segment. The solid line is drawn using the expression $l_p = 0.4 \log(l/l_p)^{0.19}$, and the dashed lines using $l_p = 0.4 \log(l/l_p)^{0.19\pm.1}$. (*b*) Average end-to-end distance. The red points are the values of $\langle r^2 \rangle$ obtained from the simulations shown in Fig. 6, *top*, using $l_p = 0.4$ nm and $d_\alpha = 0.4$ nm. The green points are the values of $\langle r^2 \rangle$ obtained from the SAXS data summarized by Kohn et al. (38) using $\langle r^2 \rangle = 6 \langle R_g^2 \rangle$, which was tested to be accurate within $\pm 1\%$ for our simulated excluded volume chains. The solid red line is drawn using a linear least-squares fit to the simulated points: $\log \langle r^2 \rangle = 1.30 \log n + 2.68$ and extrapolating the calculated values to the longer chain lengths.

relaxation time for dihedral angle rotations and thereby slow the diffusion of the chain ends, as observed.

In the classic picture described by Flory, the excluded volume of the chain must be compensated by attractive interactions in a solvent in which the chain behaves as an ideal Gaussian chain. It appears that in the absence of denaturant, interactions within our model peptide are nearly sufficient to reproduce this behavior. If this is true, then the introduction of more hydrophobic residues in the sequence should produce chains that are more compact than Gaussian chains. These are important targets for future studies.

In closing we note that the values for both k_R and D/η are sensitive to the detailed description $P(r)$. One knows a priori that the wormlike chain provides only a qualitative picture of the end-to-end distribution for these peptides. In previous work, we showed that the end-to-end distributions obtained from this model were quite similar to those obtained from

Langevin molecular dynamics simulations in the absence of any intramolecular interactions that model the fully swollen peptides in atomistic detail. Although the introduction of excluded volume appears to provide a reasonably accurate picture of the measured chain dynamics in 6 M GdmCl and 8 M urea, it is also clear that the model omits features that must be present in real chains. Most notable is the absence of any solvent ''cage'' and van der Waals effects on the probability of close contact between the two terminal residues, as seen in molecular dynamics simulations in water (64,65) as well as similar effects between other residues. Additional studies of peptides that include bulky side chains and/or specific side chain-side chain interactions using the approach described here may provide further insight into the factors that determine the apparent end-to-end diffusion coefficient and persistence length of short peptides.

REFERENCES

1. Eaton, W. A., V. Munoz, S. J. Hagen, G. S. Jas, L. J. Lapidus, E. R. Henry, and J. Hofrichter. 2000. Fast kinetics and mechanisms in protein folding. *Annu. Rev. Biophys. Biomol. Struct.* 29:327–359.

2. Lapidus, L. J., W. A. Eaton, and J. Hofrichter. 2000. Measuring the rate of intramolecular contact formation in polypeptides. *Proc. Natl. Acad. Sci. USA.* 97:7220–7225.

3. Lapidus, L. J., P. J. Steinbach, W. A. Eaton, A. Szabo, and J. Hofrichter. 2002. Effects of chain stiffness on the dynamics of loop formation in polypeptides. Appendix: Testing a one-dimensional diffusion model for peptide dynamics. *J. Phys. Chem. B.* 106:11628–11640.

4. Gonnelli, M., and G. B. Strambini. 1995. Phosphorescence lifetime of tryptophan in proteins. *Biochemistry.* 34:13847–13857.

5. Buscaglia, M., B. Schuler, L. J. Lapidus, W. A. Eaton, and J. Hofrichter. 2003. Kinetics of intramolecular contact formation in a denatured protein. *J. Mol. Biol.* 332:9–12.

6. Buscaglia, M., J. Kubelka, L. J. Lapidus, W. A. Eaton, and J. Hofrichter. 2005. Determination of ultrafast protein folding rates from loop formation dynamics. *J. Mol. Biol.* 347:657–664.

7. Lapidus, L. J., W. A. Eaton, and J. Hofrichter. 2001. Dynamics of intramolecular contact formation in polypeptides: distance dependence of quenching rates in a room-temperature glass. *Phys. Rev. Lett.* 87: 258101.

8. Wilemski, G., and M. Fixman. 1974. Diffusion-controlled intrachain reactions of polymers 1. Theory. *J. Chem. Phys.* 60:866–877.

9. Bicout, D. J., and A. Szabo. 1997. First passage times, correlation functions, and reaction rates. *J. Chem. Phys.* 106:10292–10298.

10. Szabo, A., K. Schulten, and Z. Schulten. 1980. 1st passage time approach to diffusion controlled reactions. *J. Chem. Phys.* 72:4350–4357.

11. Camacho, C. J., and D. Thirumalai. 1995. Modeling the role of disulfide bonds in protein-folding: entropic barriers and pathways. *Proteins.* 22:27–40.

12. Thirumalai, D. 1999. Time scales for the formation of the most probable tertiary contacts in proteins with applications to cytochrome *c*. *J. Phys. Chem. B.* 103:608–610.

13. Flory, P. J. 1969. Statistical Mechanics of Chain Molecules. Interscience Publishers, New York.

14. Doi, M. E. S. F. 1986. The Theory of Polymer Dynamics. Clarendon Press, Oxford.

15. Friedman, B., and B. Oshaughnessy. 1989. Theory of polymer cyclization. *Phys. Rev. A.* 40:5950–5959.

16. Friedman, B., and B. O'Shaughnessy. 1993. Theory of intramolecular reactions in polymeric liquids. *Macromolecules.* 26:4888–4898.

17. Podtelezhnikov, A., and A. Vologodskii. 1997. Simulations of polymer cyclization by Brownian dynamics. *Macromolecules.* 30:6668–6673.

18. Dua, A., and B. J. Cherayil. 2002. The dynamics of chain closure in semiflexible polymers. *J. Chem. Phys.* 116:399–409.

19. Debnath, P., and B. J. Cherayil. 2004. Dynamics of chain closure: Approximate treatment of nonlocal interactions. *J. Chem. Phys.* 120: 2482–2489.

20. Robinson, D. R., and W. P. Jencks. 1965. The effect of compounds of the urea-guanidinium class on the activity coefficient of acetyltetra-glycine ethyl ester and related compounds. *J. Am. Chem. Soc.* 87:2462–2470.

21. Chan, H. S., and K. A. Dill. 1989. Intrachain loops in polymers: effects of excluded volume. *J. Chem. Phys.* 90:492–509.

22. Lakowicz, J. R. 1999. Principles of Fluorescence Spectroscopy, 2nd ed. Kluwer Academic Publishers, Norwell, MA.

23. Chen, R. F. 1968. Dansyl labeled proteins: Determination of extinction coefficient and number of bound residues with radioactive dansyl chloride. *Anal. Biochem.* 25:412–416.

24. Kratky, O., and G. Porod. 1949. Röntgenuntersuchung gelöster Fadenmoleküle. *Recl. Trav. Chim. Pays-Bas.* 68:1106–1123.

25. Hagerman, P. J., and B. H. Zimm. 1981. Monte-Carlo approach to the analysis of the rotational diffusion of wormlike chains. *Biopolymers.* 20:1481–1502.

26. Zhou, H. X. 2002. Dimensions of denatured protein chains from hydrodynamic data. *J. Phys. Chem. B.* 106:5769–5775.

27. Domb, C. G. J.; Welmers, G. 1965. Proc. Phys. Soc. (London) 85,:625.

28. Leguillou, J. C., and J. Zinnjustin. 1977. Critical exponents for N-vector model in 3 dimensions from field-theory. *Phys. Rev. Lett.* 39:95–98.

29. Bent, D. V., and E. Hayon. 1975. Excited state chemistry of aromatic amino acids and related peptides. III. Tryptophan. *J. Am. Chem. Soc.* 97:2612–2619.

30. Qiu, L. L., and S. J. Hagen. 2004. Internal friction in the ultrafast folding of the tryptophan cage. *Chem. Phys.* 307:243–249.

31. Cowan, P. M. M., S. 1955. Structure of poly-l-proline. Nature. 176:501–503.

32. Schuler, B., E. A. Lipman, P. J. Steinbach, M. Kumke, and W. A. Eaton. 2005. Polyproline and the ''spectroscopic ruler'' revisited with single-molecule fluorescence. *Proc. Natl. Acad. Sci. USA.* 102:2754–2759.

33. Descloizeaux, J. 1980. Short-range correlation between elements of a long polymer in a good solvent. *J. Phys. [E].* 41:223–238.

34. Martin, J. L. S., M. F.; Hioe, F. T. 1967. *J. Chem. Phys.* 46:3478–3481.

35. Chan, H. S., and K. A. Dill. 1990. The effects of internal constraints on the configurations of chain molecules. *j. chem. phys.* 92:3118–3135.

36. Smith, C. R., N. Mateljevic, and B. E. Bowler. 2002. Effects of topology and excluded volume on protein denatured state conforma-tional properties. *Biochemistry.* 41:10173–10181.

37. Millet, I. S., S. Doniach, and K. W. Plaxco. 2002. Toward a taxonomy of the denatured state: Small angle scattering studies of unfolded proteins. *Adv. Protein Chem.* 62:241–262.

38. Kohn, J. E., I. S. Millett, J. Jacob, B. Zagrovic, T. M. Dillon, N. Cingel, R. S. Dothager, S. Seifert, P. Thiyagarajan, T. R. Sosnick, M. Z. Hasan, V. S. Pande, I. Ruczinski, S. Doniach, and K. W. Plaxco. 2004. Random-coil behavior and the dimensions of chemically unfolded proteins. *Proc. Natl. Acad. Sci. USA.* 101:12491–12496.

39. Goldenberg, D. P. 2003. Computational simulation of the statistical properties of unfolded proteins. *J. Mol. Biol.* 326:1615–1633.

40. Moglich, A., F. Krieger, and T. Kiefhaber. 2005. Molecular basis for the effect of urea and guanidinium chloride on the dynamics of un-folded polypeptide chains. *J. Mol. Biol.* 345:153–162.

41. Schellman, J. A. 1978. Solvent denaturation. *Biopolymers.* 17:1305–1322.

42. Schellman, J. A. 1987. Selective binding and solvent denaturation. *Biopolymers.* 26:549–559.

43. Schellman, J. A. 2002. Fifty years of solvent denaturation. *Biophys. Chem.* 96:91–101.

44. Nozaki, Y., and C. Tanford. 1971. Solubility of amino acids and 2 glycine peptides in aqueous ethanol and dioxane solutions - Establishment of a hydrophobicity scale. *J. Biol. Chem.* 246:2211–2217.

45. Nozaki, Y., and C. Tanford. 1970. Solubility of amino acids, diglycine, and triglycine in aqueous guanidine hydrochloride solutions. *J. Biol. Chem.* 245:1648–1652.

46. Tanford, C. 1970. Protein denaturation. Part C. Theoretical models for the mechanism of denaturation. *Adv. Protein Chem.* 24:1–95.

47. Tobi, D., R. Elber, and D. Thirumalai. 2003. The dominant interaction between peptide and urea is electrostatic in nature: A molecular dynamics simulation study. *Biopolymers.* 68:359–369.

48. Schellman, J. 1955. The stability of hydrogen-bonded peptide structures in aqueous solution. *Comptes Rendu Trav. Lab. Carlsberg Ser. Chim.* 29:230–259.

49. Privalov, P. L. 1997. Thermodynamics of protein folding. *J. Chem. Thermodyn.* 29:447–474.

50. Thompson, J. B., H. G. Hansma, P. K. Hansma, and K. W. Plaxco. 2002. The backbone conformational entropy of protein folding: Experimental measures from atomic force microscopy. *J. Mol. Biol.* 322:645–652.

51. Krieger, F., A. Moglich, and T. Kiefhaber. 2005. Effect of proline and glycine residues on dynamics and barriers of loop formation in polypeptide chains. *J. Am. Chem. Soc.* 127:3346–3352.

52. Huang, F., and W. M. Nau. 2003. A conformational flexibility scale for amino acids in peptides. *Angew. Chem. Int. Ed. Engl.* 42:2269–2272.

53. Schuler, B., E. A. Lipman, and W. A. Eaton. 2002. Probing the free-energy surface for protein folding with single-molecule fluorescence spectroscopy . *Nature.* 419:743–747.

54. Karplus, M., and D. L. Weaver. 1979. Diffusion-collision model for protein folding. *Biopolymers.* 18:1421–1437.

55. Karplus, M., and D. L. Weaver. 1976. Protein-folding dynamics. *Nature.* 260:404–406.

56. Islam, S. A., M. Karplus, and D. L. Weaver. 2002. Application of the diffusion-collision model to the folding of three-helix bundle proteins. *J. Mol. Biol.* 318:199–215.

57. Islam, S. A., M. Karplus, and D. L. Weaver. 2004. The role of sequence and structure in protein folding kinetics: The diffusion-collision model applied to proteins L and G. *Structure.* 12:1833–1845.

58. Buckler, D. R., E. Haas, and H. A. Scheraga. 1995. Analysis of the structure of ribonuclease A in native and partially denatured states by time-resolved nonradiative dynamic excitation energy transfer between site-specific extrinsic probes. *Biochemistry.* 34:15965–15978.

59. Hagen, S. J., J. Hofrichter, and W. A. Eaton. 1996. Geminate rebinding and conformational dynamics of myoglobin embedded in a glass at room temperature. *J. Phys. Chem.* 100:12008–12021.

60. Hagen, S. J., J. Hofrichter, A. Szabo, and W. A. Eaton. 1996. Diffusion-limited contact formation in unfolded cytochrome c: estimating the maximum rate of protein folding. *Proc. Natl. Acad. Sci. USA.* 93:11615–11617.

61. Young, W. S., and C. L. Brooks. 1996. A microscopic view of helix propagation: N and C-terminal helix growth in alanine helices. *J. Mol. Biol.* 259:560–572.

62. Hermans, J., A. G. Anderson, and R. H. Yun. 1992. Differential helix propensity of small apolar side-chains studied by molecular-dynamics simulations. *Biochemistry.* 31:5646–5653.

63. Thompson, P. A., V. Munoz, G. S. Jas, E. R. Henry, W. A. Eaton, and J. Hofrichter. 2000. The helix-coil kinetics of a heteropeptide. *J. Phys. Chem. B.* 104:378–389.

64. Yeh, I. C., and G. Hummer. 2002. Peptide loop-closure kinetics from microsecond molecular dynamics simulations in explicit solvent. *J. Am. Chem. Soc.* 124:6563–6568.

65. Portman, J. J. 2003. Non-Gaussian dynamics from a simulation of a short peptide: Loop closure rates and effective diffusion coefficients. *J. Chem. Phys.* 118:2381–2391.